Supporting Information for

High-Temperature High-Pressure Electrochemical Hydrogenation of Biocrude Oil

Primavera Pelosin[1], Francesco Longhin[2], Nikolaj Bisgaard Hansen[1], Paolo Lamagni[3], Emil Drazevic[1], Patricia Benito[4], Konstantinos Anastasakis[1], and Jacopo Catalano[*, 1]

[1.] Department of Biological and Chemical Engineering, Aarhus University, Aabogade 40, DK-8200 Aarhus N, Denmark

[2.] Department of Physics, Technical University of Denmark, Fysikvej, DK-2800 Kgs. Lyngby, Denmark

[3] Advanced Surface Plating ApS, Axel Gruhns Vej 3 8270 Højbjerg, Denmark

[4.] Department of Industrial Chemistry "Toso Montanari", Viale del Risorgimento 4, 40136, Bologna, Italy

[*] Corresponding author: Jacopo Catalano jcatalano@au.dk

13 # Composition of the pristine bio-crude oil

14

15 **Table S1** Composition of the pristine bio-crude oil tested in this work.

	RT (min)	Identified compound	Peak area (%)
1	8.24	Propanal, 2-methyl-	2.02%
2	9.16	Propane, 2,2-dimethoxy-	5.23%
3	9.64	Ethanamine, 2-(methylthio)-	1.14%
4	12.00	2,2-Dimethoxybutane	1.51%
5	12.34	Toluene	1.88%
6	13.25	1H-Tetrazole, 1-methyl-	3.09%
7	14.90	Cyclopentanone, 2-methyl-	1.69%
8	14.90	1H-Tetrazole, 1,5-dimethyl-	1.57%
9	15.16	Cyclopentanone, 3-methyl-	1.10%
10	16.64	2,7-Nonadien-5-one, 4,6-dimethyl-	0.47%
11	16.88	1,1-Dimethoxycyclopentane	1.34%
12	17.04	3-Butyn-2-one	4.68%
13	17.04	2-Cyclopenten-1-one, 2-methyl-	10.57%
14	18.12	2-Cyclopenten-1-one, 3,4-dimethyl-	1.52%
15	18.28	Cyclopentanone, 2-ethyl-	1.26%
16	18.56	4-Ethyl-4-heptanol	0.33%
17	18.98	3-Ethylcyclopentanone	1.20%
18	19.12	2-Cyclopenten-1-one, 3-methyl-	1.60%
19	19.31	Phenol	2.18%
20	19.90	Cyclobutanone, 2-(1,1-dimethylethyl)-	0.21%
21	20.05	Ethanone, 1-(2-furanyl)-	1.42%
22	20.18	2-Cyclopenten-1-one, 2,3-dimethyl-	7.31%
23	20.18	2-Oxo-2,3-dihydro-1H-imidazole-4-carbonitrile	1.27%
24	20.30	1H-Imidazole, 1-methyl-	0.90%
25	20.38	3-Heptene, 4-ethyl-	0.26%
26	20.58	Cyclohexane, 1,1-dimethoxy-	0.84%
27	21.07	Bicyclo[2.2.2]octane, 2-methyl-	0.75%
28	21.18	Benzene, 1-methyl-3-(1-methylethyl)-	0.94%
29	21.25	Ethanone, 1-(2-methyl-1-cyclopenten-1-yl)-	0.51%
30	21.36	Dimethylphosphinic fluoride	1.25%
31	21.36	3,4-dimethylfuran	1.25%
32	21.58	1,2,4,5-Tetrazine, 1,4-dihydro-3,6-dimethyl-	0.65%
33	21.83	Cyclohexanecarboxylic acid, 4-pentyl-, 4-methoxyphenyl ester, trans-	0.32%
34	22.04	5-(4-Methyl-2-nitro-phenoxymethyl)-furan-2-carboxylic acid amide	0.82%
35	22.04	2-Cyclohexen-1-one, 3,4-dimethyl-	0.90%
36	22.05	Succinic acid, ethyl 2-norbornyl ester	0.39%

Continues on next page

	RT (min)	Identified compound	Peak area (%)
37	22.29	2-Cyclopenten-1-one, 3,4,5-trimethyl-	1.79%
38	22.58	p-Cresol	0.41%
39	22.88	2-Cyclopenten-1-one, 3-ethyl-	0.44%
40	23.00	5-t-Butyl-4-methylimidazole	0.27%
41	23.21	1H-Imidazole-4-carboxaldehyde	2.55%
42	23.24	Pyridine	0.95%
43	23.25	Cyclohexene, 4-bromo-	4.84%
44	23.26	Phenol, 2-methoxy-	7.16%
45	23.61	5-Ethyl-2-furaldehyde	1.73%
46	23.62	Furan, 2,3,5-trimethyl-	1.62%
47	23.63	7-Oxabicyclo[4.1.0]heptan-2-one	0.23%
48	23.98	3-Cyclohexen-1-one, 3,5,5-trimethyl-	0.15%
49	24.11	1-(2,4-Dimethyl-furan-3-yl)-ethanone	0.27%
50	24.15	2-Isopropylimidazole	0.40%
51	24.16	Benzofuran, 2-methyl-	1.07%
52	24.59	2-Amino-4-methylpyrimidine	1.00%
53	24.60	1H-Isoindole, 2,3,3a,4,7,7a-hexahydro-	0.29%
54	24.72	3-Heptyne, 5-methyl-	0.28%
55	25.20	3,4,5-Trimethylpyrazole	0.59%
56	25.51	Phenol, 4-ethyl-	1.77%
57	25.55	Naphthalene, 1,2-dihydro-	0.21%
58	25.89	endo-2-Methylbicyclo[3.3.1]nonane	0.13%
59	26.11	2-Methoxy-5-methylphenol	0.21%
60	26.41	Hex-4-yn-3-one	0.35%
61	26.49	2-Cyclopenten-1-one, 2,3,4,5-tetramethyl-	0.96%
62	26.55	1-Pentanone, 1-(2-furanyl)-	0.38%
63	27.15	1H-Benzimidazole, 5,6-dimethyl-	0.18%
64	28.87	Octatriene, 1,3-trans-5-trans-	0.22%
65	29.00	N-(4-Fluorobenzyl)-N-methylhexadecan-1-amine	1.41%
66	29.00	Phenol, 4-ethyl-2-methoxy-	3.72%

16

17

Table S2 Composition of the pristine process water tested in this work.

	RT (min)	Identified compound	Peak area (%)
1	7.15	Butanoic acid, methyl ester	0.44%
2	8.92	Cyclopentanone	1.90%
3	9.53	Monomethyl malonate	0.53%
4	10.02	2-Cyclopenten-1-one	1.65%
5	10.31	Cyclopentanone, 2-methyl-	0.33%
6	11.93	Methyl acetoxyacetate	7.71%
7	12.21	2-Cyclopenten-1-one, 2-methyl-	4.86%
8	12.38	Butyrolactone	0.50%
9	12.85	Diisopropyl ether	10.21%
10	14.12	2-Cyclopenten-1-one, 3-methyl-	2.39%
11	14.91	Butanoic acid, 2-oxo-, methyl ester	5.35%
12	15.00	1-(3H-Imidazol-4-yl)-ethanone	0.92%
13	15.03	Methyl 2-ethoxyacetate	17.25%
14	15.14	2-Cyclopenten-1-one, 2,3-dimethyl-	1.10%
15	15.44	Malonic acid, dihydrazide	0.78%
16	15.65	Neopentane	3.87%
17	15.88	1-Propanol, 2-(2-hydroxypropoxy)-	2.32%
18	15.97	Butanedioic acid, dimethyl ester	1.86%
19	17.01	Butanedioic acid, methyl-, dimethyl ester	0.30%
20	17.72	2-Cyclopenten-1-one, 3-ethyl-	0.42%
21	18.44	5-Ethyl-2-furaldehyde	0.24%
22	19.26	Pentanedioic acid, dimethyl ester	0.41%
23	19.83	Carbonic acid, methyl phenyl ester	1.70%
24	21.34	Pyridine, 3-methoxy-	0.56%
25	21.87	Carbonic acid, methyl 4-methylphenyl ester	0.25%
26	23.18	Acetic acid, (acetyloxy)-	0.79%
27	25.64	1-(2-Methoxy-1-methylethoxy)-2-propanol, TMS derivative	0.78%
28	25.81	Benzeneacetic acid, 4-methoxy-, methyl ester	2.09%
29	25.84	Guaiacol, O-methoxycarbonyl-	2.67%
30	25.86	Paraldehyde	1.26%
31	26.08	Methyl glyoxylate oxime	2.51%
32	26.44	Cyclohexane, 1-ethyl-2-methyl-, cis-	0.34%
33	26.45	Propanoic acid, 2-methyl-, anhydride	1.64%
34	26.68	3-Nonen-2-one	0.24%
35	27.01	Benzoic acid, 2,5-dihydroxy-, methyl ester	0.23%
36	28.14	1,2-Benzenediol, O-methoxycarbonyl-O'-propoxycarbonyl-	1.55%
37	28.14	1-Aminocyclopentanecarboxylic acid, N-(allyloxycarbonyl)-, pentyl ester	1.55%

Continues on next page

	RT (min)	Identified compound	Peak area (%)
38	28.52	2-Methoxy-5-methylphenol, O-methoxycarbonyl-	0.24%
39	29.39	2,5,8,11-Tetraoxadodecane	1.33%
40	30.02	6-Undecanol	0.52%
41	30.30	1,2-Benzenediol, O,O'-di(methoxycarbonyl)-	4.40%
42	30.58	Benzeneacetic acid, 3,4-dimethoxy-, methyl ester	1.32%
43	31.11	2,6-Dimethoxyphenol, O-methoxycarbonyl-	1.49%
44	32.04	2-Fluorobenzoic acid, 4-nitrophenyl ester	2.88%
45	32.52	2-Aminocaprylic acid, N-allyloxycarbonyl-, butyl ester	0.27%
46	32.71	Benzeneacetic acid, 4-hydroxy-3,5-dimethoxy-, methyl ester	0.15%
47	33.04	Fumaric acid, dipropargyl ester	0.35%
48	33.66	Ethanol, 2-[4-(1,1-dimethylethyl)-2-methylphenoxy]-	1.14%
49	33.72	3-(2,3,4-Trimethoxyphenyl)propionic acid	0.42%
50	35.38	Furane-3-carbohydrazide, 5-tert-butyl-2,N2,N2-trimethyl-	0.28%
51	35.44	Ethanone, 1-(3,4,5-trimethoxyphenyl)-	1.29%
52	36.56	Benzamide, 3,4,5-trimethoxy-N-(2-benzyloxyethyl)-	0.42%

Electrochemical set-up

Ambient pressure set-up

Ambient pressure experiments were performed in an H-cell (see Figure S1a) which allowed for measuring the pressure increase as well as the local production of hydrogen. The working (WE) and the reference electrodes (RE) were placed close together in the cathodic compartment. The counter electrode (CE) was placed in the anodic compartment, and immersed in an aqueous buffered solution (carbonate buffer 1 M pH 8.77). Half-cell (WE-RE) and the total cell potential (WE-CE) were continuously monitored.

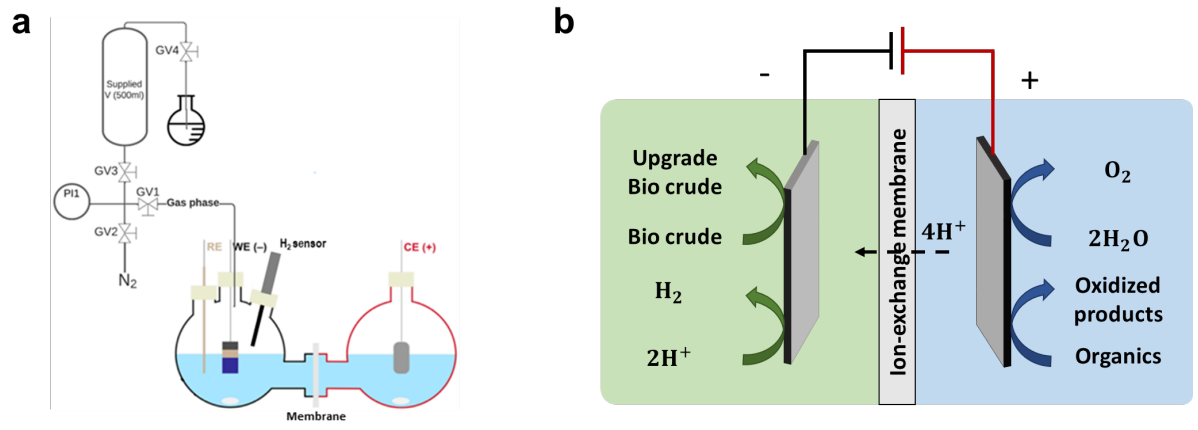

Figure S1 a Schematic of the H-cell used for online measurement of pressure and local hydrogen produced and **b** electrochemical paths.

The cathodic compartment was directly connected to a 500 mL reservoir (stainless steel 316L, Swagelok), which acted as an expansion chamber to decrease the overall pressure. The pressure was monitored via a pressure transducer (PI1, UNIK 5000 full scale 1 bar(g)), while the local hydrogen concentration was measured via an H_2 micro-sensor (Unisense, DK). The latter sensor, which works as a Clark electrode, was placed in the gas phase in close proximity of the gas-liquid interface. While the sensor can be used to measure H_2 concentration both in the liquid and gas phases, we decided to monitor the H_2 concentration in the gas phase to avoid contamination in the electrolyte solution inside the sensor and to decrease its response time (below 1s). Here we note that we have used the H_2 concentration as an indication of the presence of some parasitic electrochemical reactions (*i.e.* hydrogen evolution reaction, HER) since the concentration as read from the sensor is not representative of the average H_2 concentration in the system due to the long diffusive path (from the gas-liquid interface to the upper part of the expansion cylinder) and stagnant conditions. The system was tested against pressure leak; due to the relatively large expansion volume used, the measured leak under similar conditions to the one used in CA was below $2 \cdot 10^{-2}$ Pa s^{-1} at 1.3 bar absolute pressure. The temperature was monitored with a thermometer which allowed us to perform accurate measurement of the moles of gas produced during the electrolysis. The total volume of the

system (including reservoir, fittings and tubing) was calculated from water splitting experiments (2 hours) by comparing the theoretical moles of H_2 produced from the charge measured during electrolysis with the ones calculated from the pressure increase in the system and the ideal gas law. The total volume of the cathodic side of the two-cell compartment (gas head space plus liquid space) was measured as 547.3 mL.

All the fitting, valves and tubing were bought from Swagelok. All the signals (pressure, H_2 concentration, half-cell voltage, and total cell-voltage) were acquired via NI-9219 acquisition cards (National Instruments) monitored and recorded with Labview at 1 Hz.

High pressure set-up

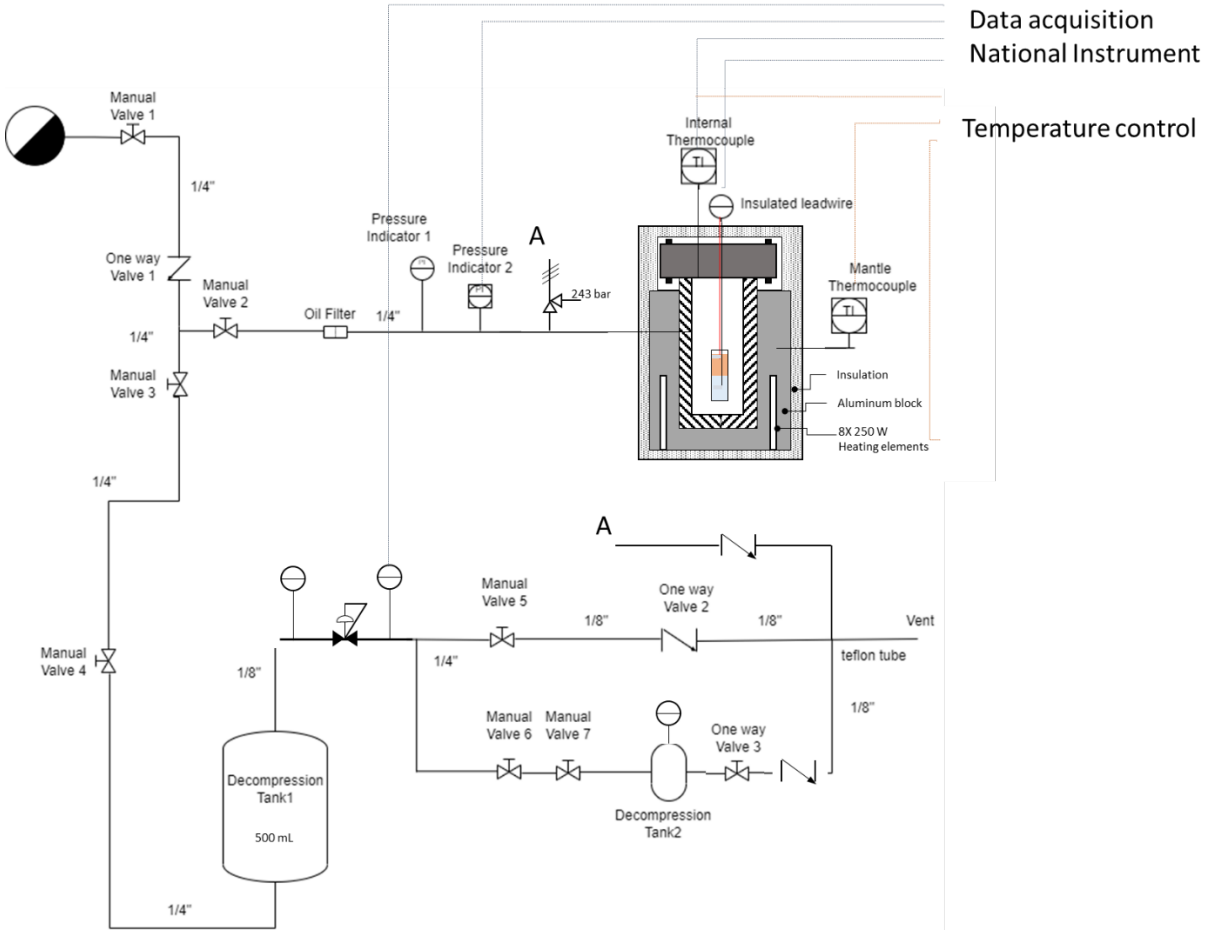

Figure S2 Schematic of the high pressure set-up used for the electrochemical characterization.

The schematic of the set-up used for high pressure electrochemical characterization is reported in Figure S2. Briefly a glass cell (dimension: internal diameter 15 mm, height 50 mm) was

fitted with the working electrode (Ni foam) and counter electrode (Ti mesh) and placed inside a reactor rated for high pressure and temperature (HIP USA, custom made: maximum temperature 426 °C max pressure 1103 bar, pressure/temperature rating 300 bar at 300 °C). The connections for the lead wires were placed on the flange of the reactor through a high-pressure fitting (Conax USA, maximum temperature 232 °C and maximum pressure 690 bar).

The temperature of the system was controlled by heating an aluminium block via 8 heating elements (250 W each, RS components). The PID control (Arduino Uno board) received the internal temperature (thermocouple type K with two isolated thermo-elements, 1/8 inch Omega) placed in a thermo-well and computed an analogic output to control the heating elements through a relay, by using a pulse width modulation (PWM) signal. This way even though the heating elements were either on or off, the regulator used the PID principles by running the heating elements on a duty cycle between 0 and 100%. An additional Arduino Uno board was used as safety measure to cut the power to the heating element if the temperature (read by an additional thermocouple type K, 1/8 inch Omega) of the aluminium block exceeded a safety limit (400 °C). The code for the temperature control was written in ArduinoIDE.

The system was pressurized with nitrogen via a lateral port on the reactor body connected to a high pressure line. This line was equipped with a safety valve (HIP, opening at 243 bar), a pressure transducer (RS components, full scale 248 bar), analogic pressure indicator (Parr Instrument, maximum reading 300 bar), and an oil filter. For depressurizing the system the reactor was also connected to an expansion vessel (Swagelok, 500 mL) and a pressure regulator (Swagelok, inlet pressure 70 bar max, outlet pressure 10 bar max). Finally, the gas head space, after being laminated below 5 bar, could either be vented or routed through a bypass line and collected in a stainless steel vessel (Parr, 25 mL reactor max operating pressure 150 bar) for further off-line analysis via gas chromatography.

All fitting and valves in the high pressure side of the set-up were in stainless steel purchased from HIP, while on the low pressure side were in 316 stainless steel and bought from Swagelok. The signals (internal pressure and temperature, cell voltage, and PWM signal) were acquired via NI-9207 acquisition cards (National Instruments) monitored and recorded with Labview at 1 Hz.

After placing the WE and CE, the cell was filled with approximately 1 g of pristine BC and 5 mL of process water. Due to the very viscous nature of the pristine BC, the oil at room temperature rested at the bottom of the cell. However, when the BC was heated up above approximately 75 °C, it had a significantly lower viscosity (1.93 $Pa \cdot s$ versus 17.2 $Pa \cdot s$ at room temperature) and an inversion of liquid phases driven by the density started to be observed. Inside the reactor it was not possible to observe this inversion directly; it was possible however to indirectly detect it electrochemically. Figure S3 reports the reference polarization curves between -3V and 1V of process water (dark blue) and pristine biocrude oil (black) together with a sample containing both BC and PW (red). These experiments were carried out by using the same glass cell as the chrono-amperometry tests by using Ti rods both as the cathode and the anode, both extending to the bottom of the cell. Both electrodes were encased in Teflon sleeves for almost their entire length, but leaving uncovered a few mm at their end (See Figure S3a). For these experiments, the cell was heated ether at 130 °C and 10 bar (Figures S3b and S3c) or at 150 °C and 10 bar (Figures S3d and S3e). Figures S3b and S3d show the results of the polarization curves for the BC+PW sample just after reaching the working temperature while Figures S3c and S3e report the data after around 30 minutes. The results at 130 °C show that when the system reached the target temperature (time 0 min) the bottom phase was still mostly BC, which is expected due to BC's high viscosity.

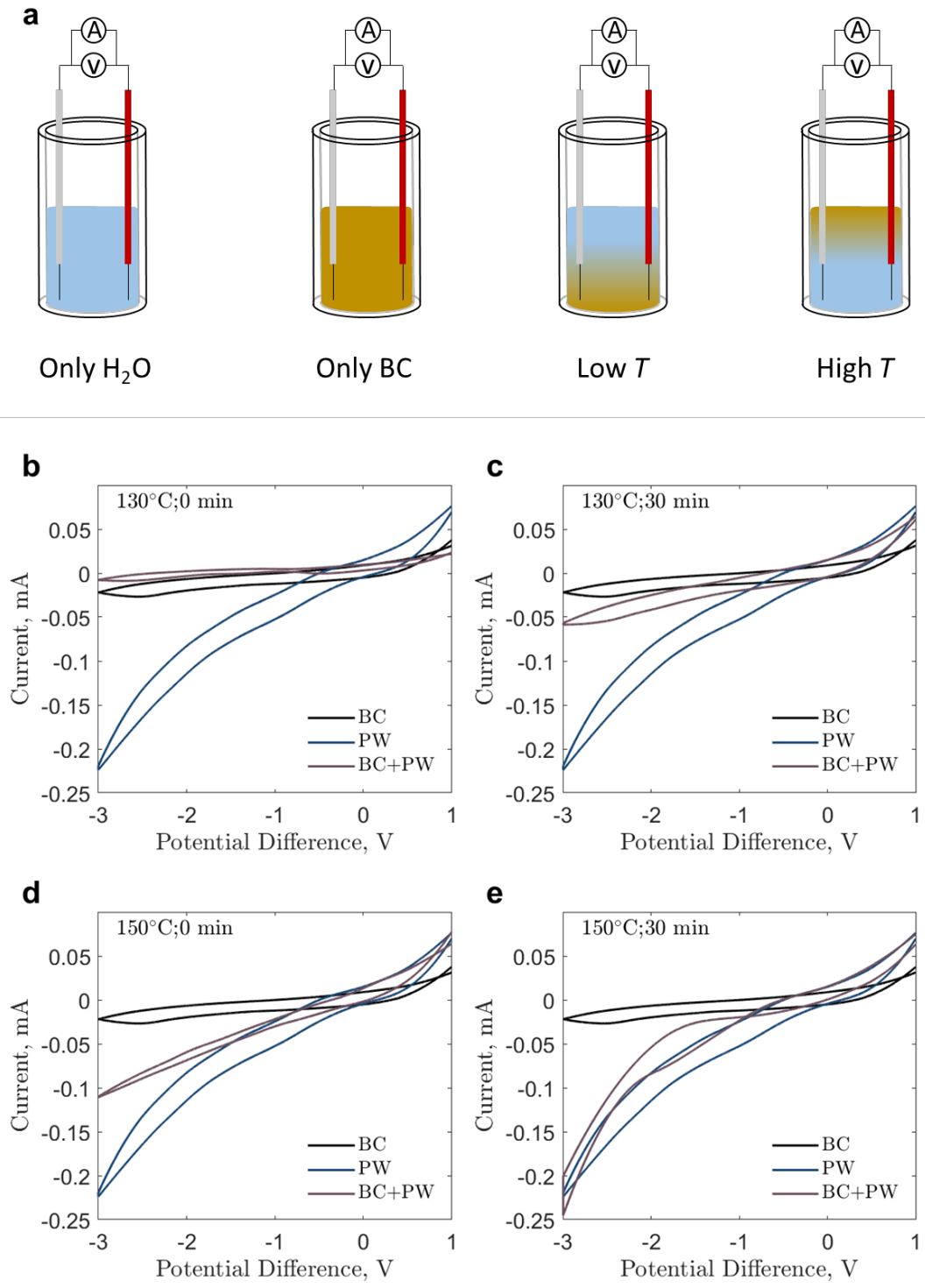

Figure S3 a Cell used in the experiment and electrical connections; **b** and **c** Polarization curves at 130°C and 10 bar. Curves of process water (dark blue) and pristine biocrude oil (black) together with a sample containing both BC and PW (dark red): **b** after reaching the target temperature and **c** after 30 minutes. **d** and **e** Polarization curves at 150°C and 10 bar. Curves of process water (dark blue) and pristine biocrude oil (black) together with a sample containing both BC and PW (dark red): **d** after reaching the target temperature and **e** after 30 minutes.

The tests were performed with an initial voltage of 1 V, high voltage of 1 V, low voltage of -3 V, scan rate of 0.05 V s^{-1}, sample interval of 0.001 V, and sensitivity of $1 \cdot 10^{-5}$ A V^{-1}.

However in this case the bottom phase must still contain a quite significant fraction of BC. Tests at 150 °C showed that at the beginning of the experiment (temperature had just reached 150 °C, time 0 min) some of the water was already present at the bottom of the cell. The switch between BC and water was then completed when the system was held for 30 minutes. The switch of position between water and BC can be explained by a decrease of the viscosity of the BC with increasing temperature, and the lower density with respect to the PW.

Electrochemical activity of biocrude – Ambient pressure tests

Ion content (ICP-OES) and ash content (TGA)

Table S3 reports the ash amount (from thermogravimetric analysis, TGA), sodium and potassium contents (from Inductively coupled plasma - optical emission spectrometry ICP-OES) and pH for different tests performed in the H-Cell at room pressure and at 60 °C. From Table S3, it is possible to notice that a small amount of K^+ (0.5-0.6 mmol/L) was detected in all the experiments independently by the separator used. We have ascribed the presence of K^+ to impurities of the buffer solution, which electro-migrated to the catholyte under working conditions.

Table S3. Ash amount, sodium content, potassium content and pH of the biocrude solutions (10 mg/mL in MeOH) treated with CEM, AEM, and BPM membranes.

Membrane	Ashes % [a]	c_{Na^+} [b] (mmol/L)	c_{K^+} [b] (mmol/L)	pH
Blank CEM [c]	14	45.3	0.0	9.3
CEM (-1 V)	16	112.2	0.5	10.5
Blank AEM [c]	/	1.6	2.8	7.6
AEM	11	8.1	0.6	8.6
Blank BPM [c]	/	2.1	0.2	6.2
BPM	4.5	3.7	0.6	8

Notes [a] Results from TGA, [b] From ICP-OES, [c] Electrochemical Blank, same conditions as in the bulk electrolysis but at the open circuit potential (*i.e.* without applying a voltage bias).

Figure S4 reports typical TGA and DTG curves for the pristine biocrude and for the product after electrolysis. A heating (N_2)-iso (N_2)-heating (air) method was used to determine the ash content of the BC residual.

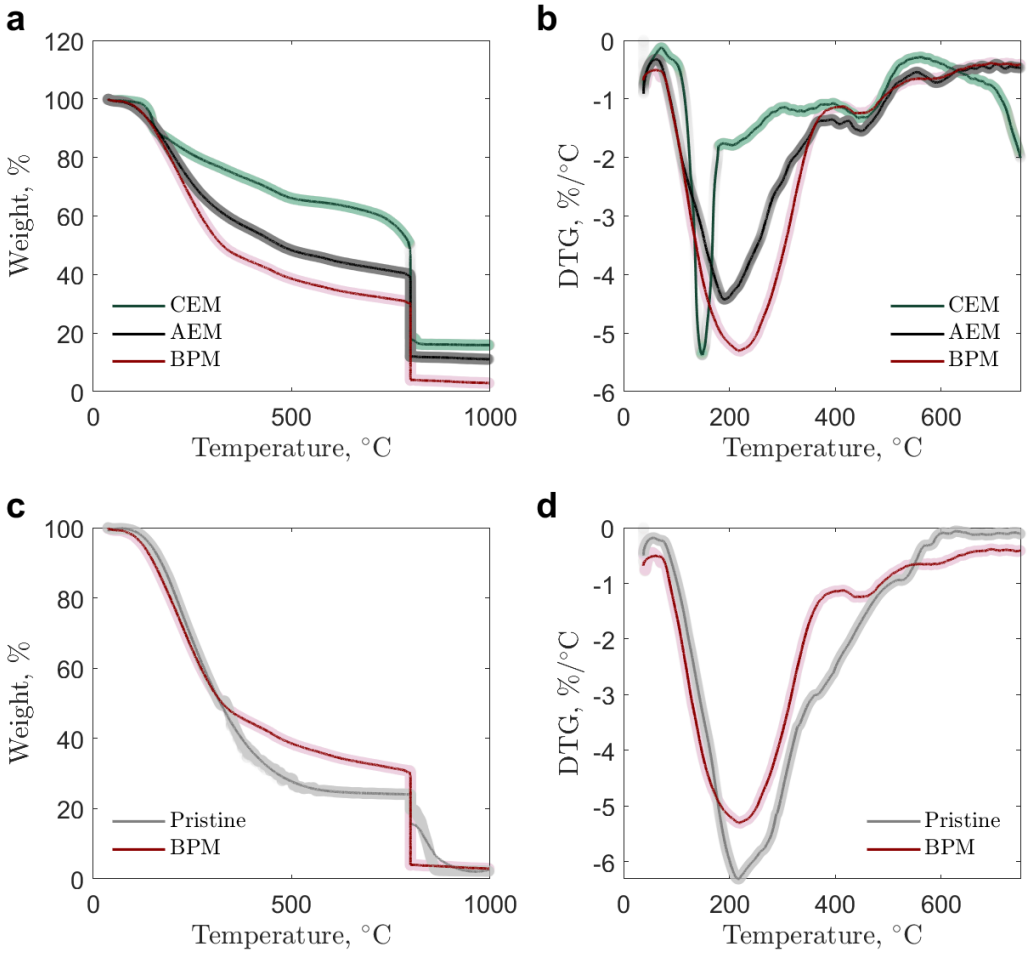

Figure S4 a TGA and **b** DTG of electrochemically treated biocrude using a CEM (green), AEM (black) and BPM (red) membrane. **c** TGA and **d** DTG of pristine (grey line) and after electrochemical treatment with BMP configuration. TGA temperature program: heating from 40 °C to 800 °C, 20 K/min, N_2 atmosphere; Isothermal step 4 hours at 800 °C, N_2 atmosphere; heating from 800 °C to 1000 °C, 20 K/min, in synthetic air (20% O_2).

Table S4 reports the observed onsets of the hydrogen evolution reaction for the tests carried out with the AEM and BPM configuration (see Figure 1 in the main text for the time-evolution profiles of the applied voltage difference at the cathode, cumulative charge, H_2 concentration, and pressure).

Table S4. H_2 evolution onset potential, charge and, time.

Membrane	Onset		
	Potential (V)	**Charge (C)**	**Time (h)**
AEM	-2.0	-1.5	8
BPM	-2.5	-52	13

FT-IR and GC-MS analysis

Table S5 reports the assigned functional groups of the FT-IR spectra. The deconvolution of the spectra reported in Figure 1 in the main text was performed by fitting the spectra with gaussian peaks in Matlab R2020b. Briefly, the spectra were divided into three main regions: 1) O-H stretching (3720–3060 cm^{-1}), 2) C-H stretching (3060–2780 cm^{-1}), and 3) finger print region (1825–1000 cm^{-1}). For the first two regions, the best fitting was performed allowing the program to iteratively adjust the position of the peak starting from a guess value. For the fingerprint region, a different approach was needed due to the large number of peaks. The fingerprint region was subdivided into three sub-regions (1825–1490 cm^{-1}, 1490–1320 cm^{-1}, and 1320–1000 cm^{-1}). A preliminary fitting was performed for each region with fixed-position peaks. Afterwards, and still keeping the position of the peaks fixed, the full fingerprint region was deconvoluted by using as guess values for the peak half-width and peak height the values found in the preliminary fitting.

To remove human bias and to allow for meaningful comparison, for all the deconvoluted spectra we kept constant the position of the peaks in the fingerprint region.

Table S5. FTIR Main bands´ frequencies and assigned functional group.

ν (cm^{-1})	Group
3418	O-H st Free Alcohols[1]
3213	O-H st Intramolecular[1]
2951	C-H st Alkanes [1]
2919	C-H st Alkanes[1]
2866	C-H st Alkanes[1]
1686	C=O st Conjugated Ketones[2]
1588	C=C st Cyclic Alkenes[2]
1516	Lignin Skeletal Vibration[2]
1456	C-H bn Alkanes[1]
1407	O-H bn Alcohols[2,3]
1274	C-O st Aryl Ethers[2,3]
1220 – 1050	C-O st Alcohols[2,3]
1033	C-O st Vinyl Ethers[4]

Table S6. GC-MS analysis: peak attribution, retention time and boiling point. The peak number refers to Figure 1f in the main text.

Peak	RT (min)	Boiling Point (°C)	Molecule
1	17.0	74	3-methylcyclopent-2-en-1-one -
2	20.2	80	2,3-dimethylcyclopent-2-en-1-one
3	21.5	80	2,3-dimethylcyclopent-2-en-1-one
4	23.2	266	2-methoxyphenol
5	29.0	235	4-ethyl-2-methoxyphenol

Preparative electrolysis with PW and biocrude

We performed preparative electrolysis with the BPM configuration by using the same step voltammetry as presented in Figure 1a in the main text.

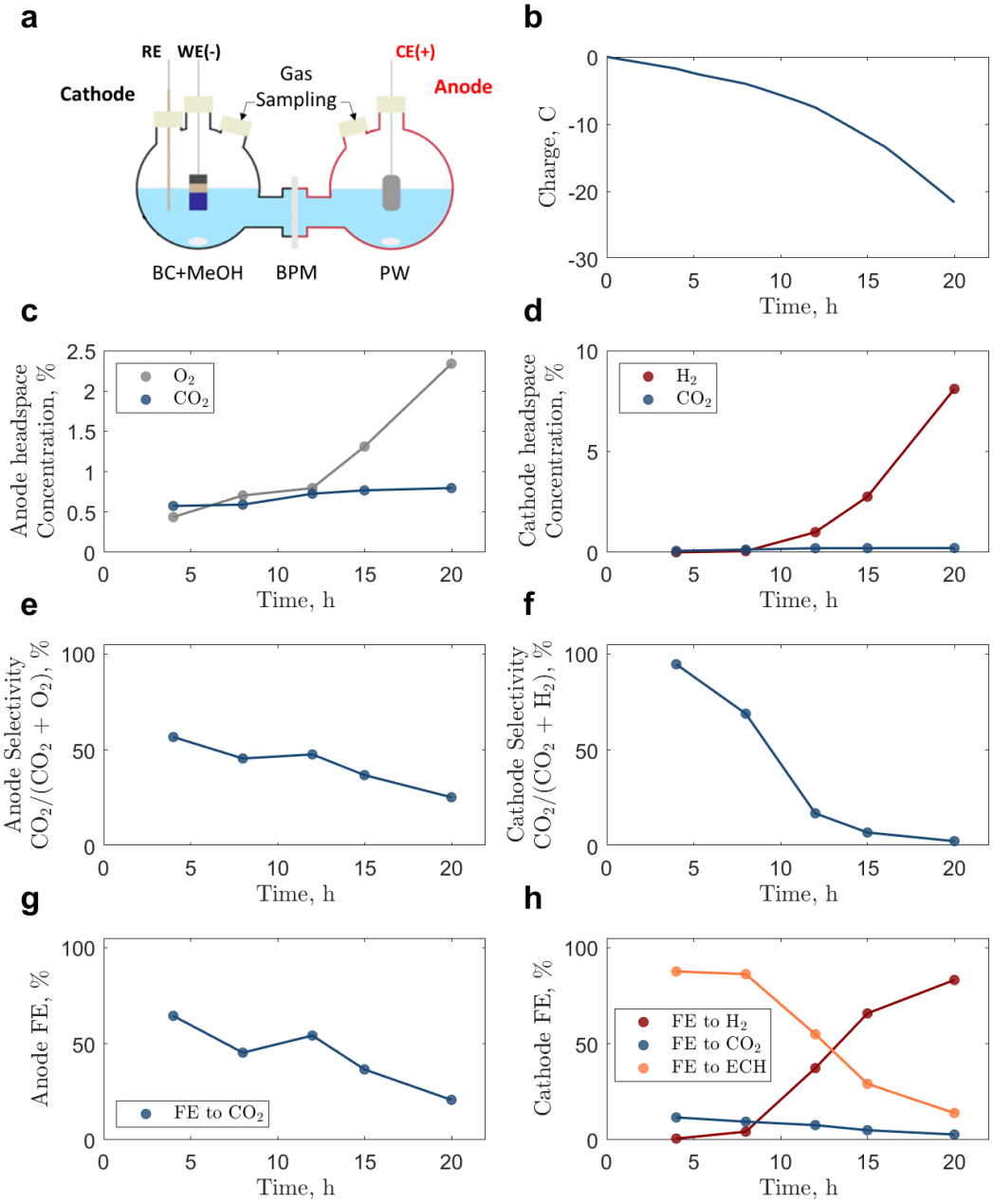

Figure S5 a Setup used for BC/methanol and PW experiment, **b** charge versus time, **c** O_2 and CO_2 concentrations at the anodic headspace, **d** H_2 and CO_2 concentrations of the cathodic headspace, **e** anode selectivity, **f** cathode selectivity, **g** calculated anodic faradaic efficiency of the electro-oxidation of PW, **h** calculated cathodic faradaic efficiency to CO_2, H_2 and ECH conversion.

Different from the ambient pressure setup reported in Figure S1, we used process water as anolyte (see Figure S5a) and we monitored the gas evolution at the anodic and cathodic headspace via sampling and gas chromatography instead of an H_2 sensor. For this experiment,

199 we did not connect the pressure sensor and to avoid overpressure we reduced of around 5 times
200 the cathode active area, resulting in a much lower current density and charge delivered to the
201 system (refer to Figure S5b and Figure 1b in the main text).
202 Figures S5c and S5d show the gas evolution in the anodic and cathodic chamber, respectively.
203 The selectivity of the CO_2 versus O_2 and H_2 is instead reported in Figure S5e and S5f, while
204 the faradaic efficiencies are reported in Figure S5g and S5h, for the anode and the cathode,
205 respectively. For the anodic compartment, an evident evolution of CO_2 is recorded in the first
206 12 hours of the experiment. This might be associated to the oxidation of organic compounds
207 present in the PW. A decrease in the CO_2 production, thus the selectivity and faradic efficiency,
208 could be observed over time. We ascribed this behaviour to the increase in the voltage bias at
209 the anode due to the current matching (see voltage profile reported in Figure 1a in the main
210 text). In any case, the substantial production of CO_2 points towards the possibility of a (partial)
211 treatment of the PW.
212 The gas composition at the cathode (Figure S5d) follows the results reported in the main text,
213 with a sharp increase of the H_2 content after around 12 hours. When comparing the cumulative
214 charge over time (Figure S5b) and the H_2 concentration evolution (Figure S5d), we can see a
215 region where the charge was increasing while the H_2 concentration remained low. This can be
216 also seen with reference to Figure S5f where we report the selectivity of CO_2 versus the total
217 gas production. As reported in the main text, these results show that until 12 hours, the electrical
218 charge is mostly used to promote reactions different from the HER. The sharp decrease in the
219 CO_2 selectivity and faradaic efficiency after 12 hours was due to the HER becoming the most
220 prominent cathodic electrochemical reaction.
221 In the case of the cathodic chamber, other different reactions not involving either HER or CO_2
222 might be present (*e.g.* direct hydrogenation). This can be seen from the calculated faradaic
223 efficiencies to H_2 and CO_2 (Figure S5h). Indeed, from the charge and GC analysis we can

estimate at 12 h (before the onset of HER) a Faradaic efficiency of ~8% to CO_2, ~37% to H_2 and the remaining 55% might be associated to ECH reactions.

Electrochemical activity of biocrude – High pressure tests

EIS results

Figure S6 shows an example of electrochemical impedance spectroscopy (EIS) performed after bulk electrolysis at 150 °C and 80 bar and 10 V applied potential difference. Impedance data were collected at the test pressure and temperature with a two-electrode set-up, thus they include also the resistances external to the electrochemical cell (*e.g.* lead wires, contact resistance etc.). The charge transfer resistance at both the anode and the cathode is clearly visible. In Figure S6a symbols represent the experimental data and the continuous curves the best fitting obtained with the equivalent electrical circuit reported in Figure S6b. More specifically, EIS data were fitted considering an ohmic resistance (R_0 which also include all the resistances of cables and contact resistances) in series with two R-CPE circuits (resistance in parallel with a constant phase element). The CPE elements were added to account for the behaviour of the double layer.

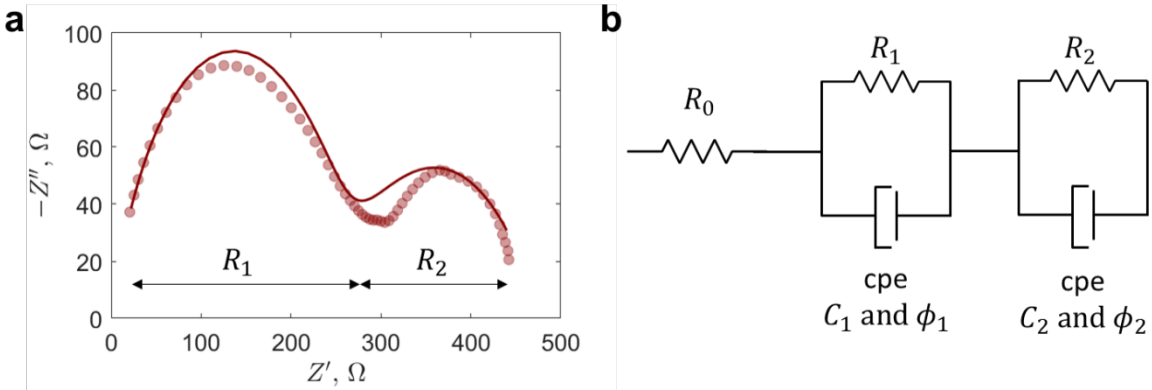

Figure S6 a Example of EIS data and **b** equivalent electrical circuit used for the data fitting reported in Figure S7. The EIS was collected in the biocrude/process water system after electrolysis performed at 150 °C and 80 bar and 10 V applied potential difference. EIS settings: -2V of bias, in the frequency range $f \in [1,10^5]$ Hz.

Figure S7 reports the experimental data before (grey) and after (red) electrolysis for experiments performed at 150 °C and 200 °C at an applied potential differences of 10V, 20V and 30V.

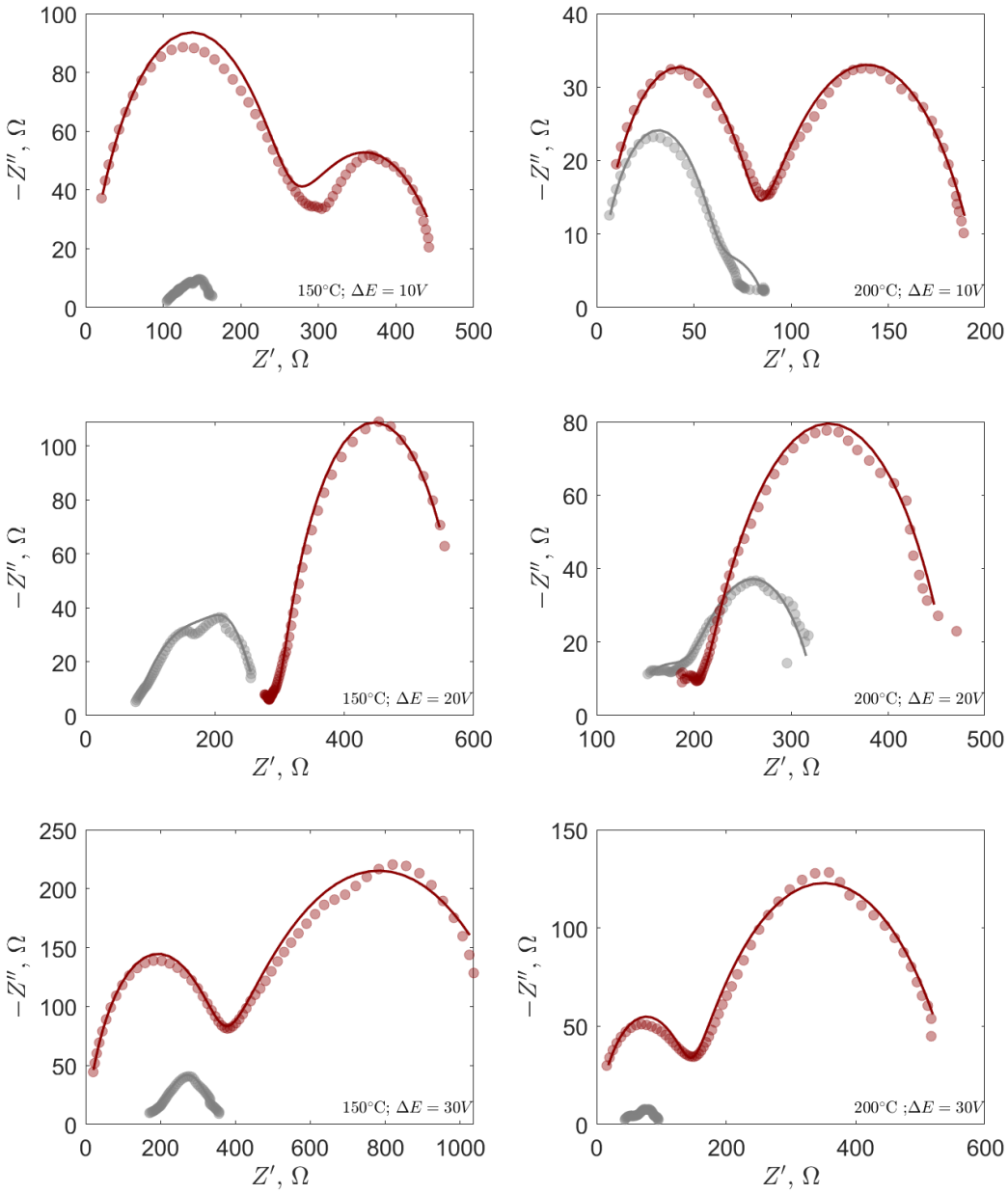

Figure S7 EIS at 150 °C (left) and at 200 °C (right) before (grey) and after (red) electrolysis of 20 minutes at 10 V, 20 V, and 30 V. Symbols represent experimental data while the continuous curves are the best fitting obtained with an equivalent circuit (see Figure S6b) containing two parallel R-CPE elements connected in series. Fitting parameters can be found in Table S7. EIS performed at –2 V of bias, in the frequency range $f \in [1,10^5]$ Hz.

The fitting, represented with solid lines, was performed with the software MEISP, and the parameters found are reported in Table S7.

Here we note that only for some tests was possible to univocally determine all the values for the equivalent electrical components. In particular the experiments before the electrolysis often show only one clear depressed semicircle (R-CPE element). Therefore, the vales of the fitting reported in Table S7 should be considered as indicative. On the other hand the fitting allows to obtain a reliable value for the total cell resistance ($R_{\mathrm{tot}} = R_0 + R_1 + R_2$).

Table S7. Parameters for the EIS fitting shown in Figure S7, refer to Figure S6b for the equivalent electrical circuit.

$\boldsymbol{\Delta E}$	$\boldsymbol{R_0}$	$\boldsymbol{R_1}$	$\boldsymbol{C_1}$	$\boldsymbol{\phi_1}$	$\boldsymbol{R_2}$	$\boldsymbol{C_2}$	$\boldsymbol{\phi_2}$
V	Ω	Ω	F	-	Ω	F	-
Before electrolysis, $T = 150$ °C							
10	$1.1 \cdot 10^{2}$	$2.6 \cdot 10^{1}$	$1.4 \cdot 10^{-4}$	0.57	$3.4 \cdot 10^{1}$	$1.2 \cdot 10^{-3}$	0.63
20	$7.4 \cdot 10^{1}$	$1.8 \cdot 10^{2}$	$4.0 \cdot 10^{-4}$	0.43	$2.0 \cdot 10^{1}$	$7.6 \cdot 10^{-4}$	1.00
30	$1.6 \cdot 10^{2}$	$1.8 \cdot 10^{2}$	$4.4 \cdot 10^{-4}$	0.34	$3.9 \cdot 10^{1}$	$4.1 \cdot 10^{-5}$	0.93
After electrolysis, $T = 150$ °C							
10	$< 10^{-3}$	$2.2 \cdot 10^{2}$	$4.2 \cdot 10^{-4}$	0.55	$2.6 \cdot 10^{2}$	$9.5 \cdot 10^{-7}$	0.77
20	$2.6 \cdot 10^{2}$	$5.2 \cdot 10^{1}$	$9.5 \cdot 10^{-4}$	0.83	$3.5 \cdot 10^{2}$	$2.5 \cdot 10^{-4}$	0.80
30	1.3	$3.4 \cdot 10^{2}$	$4.0 \cdot 10^{-7}$	0.83	$8.8 \cdot 10^{2}$	$1.4 \cdot 10^{-4}$	0.58
Before electrolysis, $T = 200$ °C							
10	$< 10^{-3}$	$5.6 \cdot 10^{1}$	$1.1 \cdot 10^{-6}$	0.85	$3.2 \cdot 10^{1}$	$1.8 \cdot 10^{-3}$	0.44
20	$1.3 \cdot 10^{2}$	$7.4 \cdot 10^{1}$	$1.3 \cdot 10^{-4}$	0.41	$1.3 \cdot 10$	$4.3 \cdot 10^{-4}$	0.65
30	$4.5 \cdot 10^{1}$	$1.0 \cdot 10^{1}$	$3.1 \cdot 10^{-6}$	0.90	$4.1 \cdot 10^{1}$	$9.6 \cdot 10^{-4}$	0.52
After electrolysis, $T = 200$ °C							
10	$< 10^{-3}$	$8.0 \cdot 10^{1}$	$7.6 \cdot 10^{-7}$	0.84	$1.2 \cdot 10^{2}$	$3.7 \cdot 10^{-4}$	0.64
20	$1.5 \cdot 10^{2}$	$6.1 \cdot 10^{1}$	$4.6 \cdot 10^{-5}$	0.43	$2.5 \cdot 10^{2}$	$1.6 \cdot 10^{-4}$	0.71
30	$< 10^{-3}$	$1.4 \cdot 10^{2}$	$8.3 \cdot 10^{-7}$	0.80	$4.2 \cdot 10^{2}$	$1.3 \cdot 10^{-4}$	0.67

A first round approximation of the conductivity of the BC at high-temperature and high-pressure conditions could be estimated from R_{tot}, the geometrical area of the electrodes, and the distance between them. Here we considered R_{tot} to be entirely due to the BC hence giving the lower-bound (minimum value) of the conductivity. This is equivalent to consider both the

resistances of the water phase and the interphase negligible with respect to the one of the BC. The results of such an analysis are reported in Figure S8. For 150 °C the BC conductivity can be estimated as: 2400 µS cm^{-1} (25% Quartile: 1800 µS cm^{-1}; 75% Quartile: 3100 µS cm^{-1}) while for 200 °C the BC conductivity is calculated as: 4700 µS cm^{-1} (25% Quartile: 2350 µS cm^{-1}; 75% Quartile: 7100 µS cm^{-1}). These results are around 40 to 80 times higher than then one measured for BC/methanol solutions at ambient conditions (reported in the main text under the section Materials and Methods).

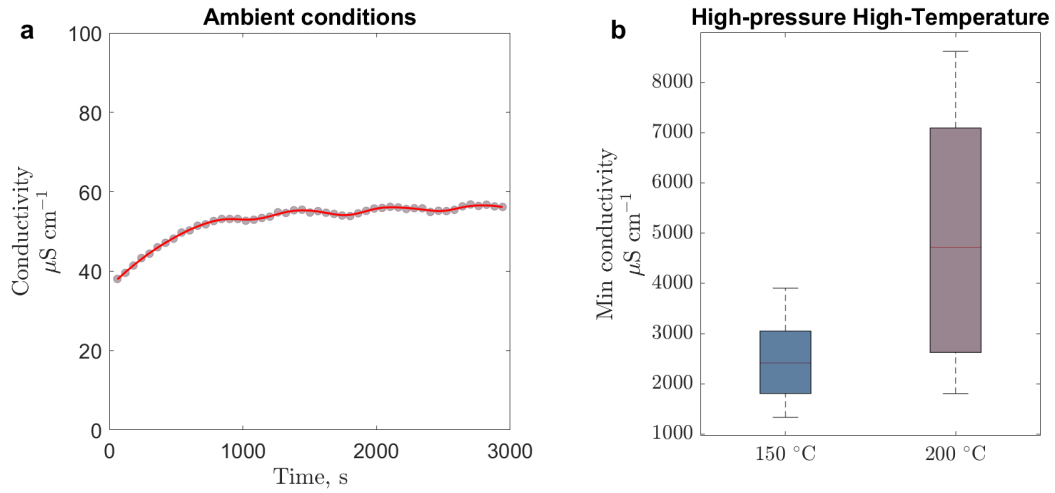

Figure S8 a Measured ionic conductivity at ambient pressure conditions and **b** estimated conductivity (from EIS data, See Figure S7) at high-pressure and high-temperature conditions.

FT-IR analysis

Figure S9 shows the IR data of the BC residue after 20 minutes electrolysis performed at 150 °C and 200 °C at an applied potential differences of 10 V, 20 V and 30 V. For the sake of comparison, Figure S9 includes also the data of the electrochemical blanks. The electrochemical blanks were performed at the same temperature, O_2 initial concentration, and the same amount of time (including heating and cooling down of the reactor) as the bulk electrolysis. Different from the electrolysis tests, during electrochemical blanks the electrodes were kept at the open circuit potential. Figure S9 reports also the deconvolution of the spectra

obtained with an identical procedure described above (section: Electrochemical activity of biocrude – Ambient pressure tests).

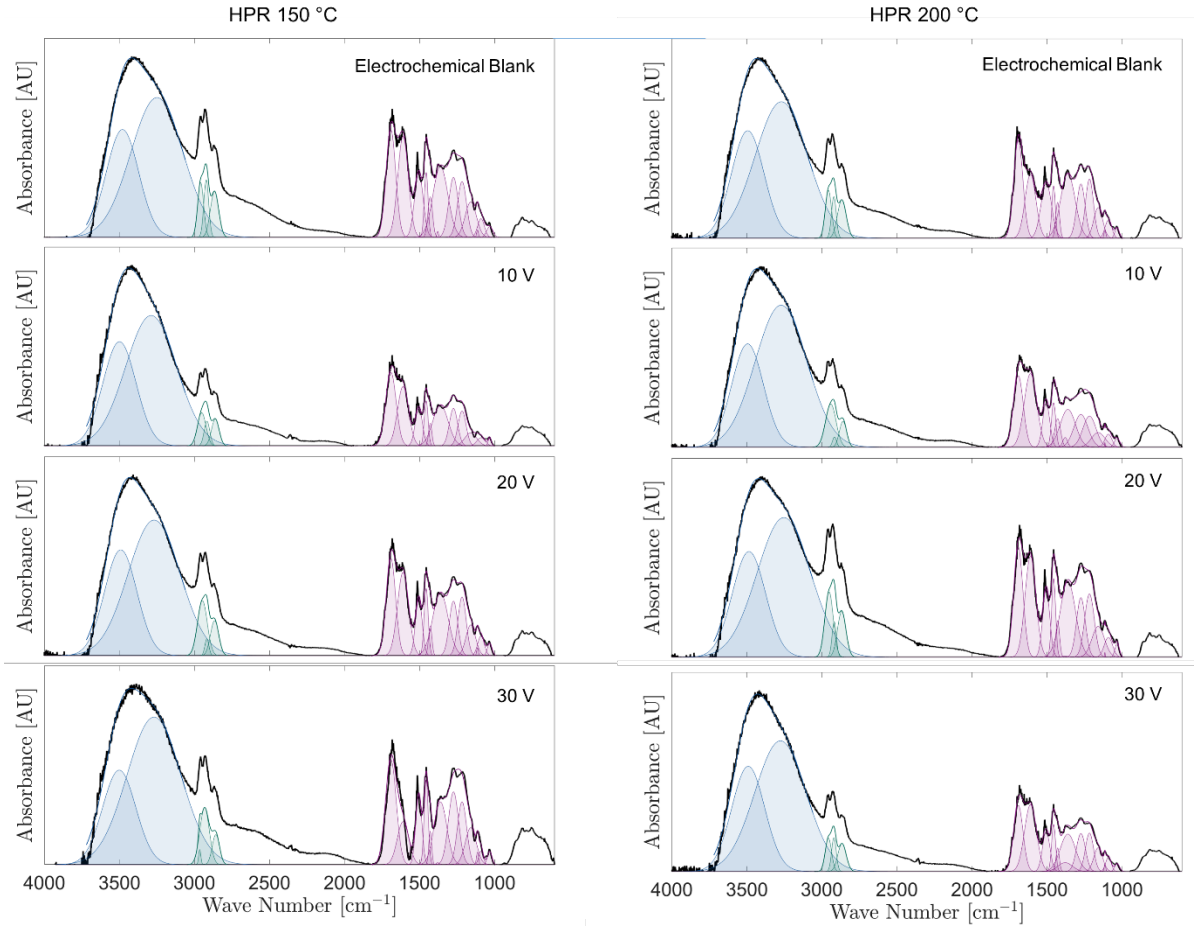

Figure S9 FTIR spectra (and deconvolution) of the biocrude thermally treated (electrochemical blank) and the biocrude electrochemically treated at 10 V, 20 V, 30 V. Left, 150 °C; right, 200 °C.

Figures S10 and S11 show the results of the deconvolution of the IR spectra collected on the BC residues after the series of electrolysis performed at 150 °C and 200 °C, respectively. For the deconvolution, we have divided the spectrum in three different regions: O-H stretching (3720–3060 cm^{-1}), C-H stretching (3060–2780 cm^{-1}), and finger print region (1825–1000 cm^{-1}). Each of these regions is colour-coded in Figure S10. The relative percentage reported in the upper panel of Figures S10 and S11 represents the ratio between the area of the specific peak and the sum of the areas of the region of the deconvolution. *E.g.* the sum of the relative percentage of the O-H stretching and O-H intramolecular is 100%. The lower panel indicates

if the peak area increased or decreased with comparison with the pristine biocrude. For the sake of comparison, both Figure S10 and S11 include the results measured for the low pressure electrochemistry with BPM.

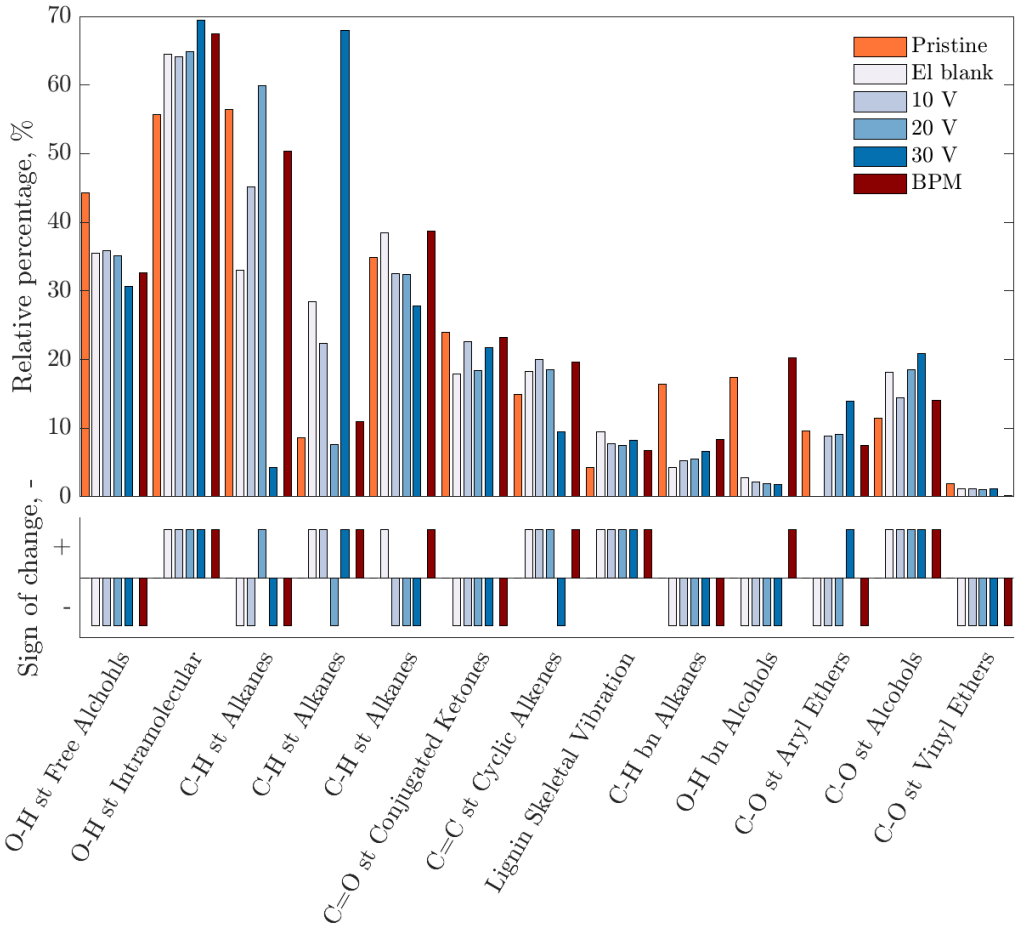

Figure S10 Upper panel: Relative percentage of the bands deconvoluted from the FTIR spectra (reported in Figure S9) of the pristine, electrochemical blank, and samples treated at 10 V, 20 V and 30 V at 150 °C. Lower panel: sign of the change with respect to the pristine BC. The deconvolution for the BPM configuration at ambient pressure and 60 °C is added for comparison (dark red).

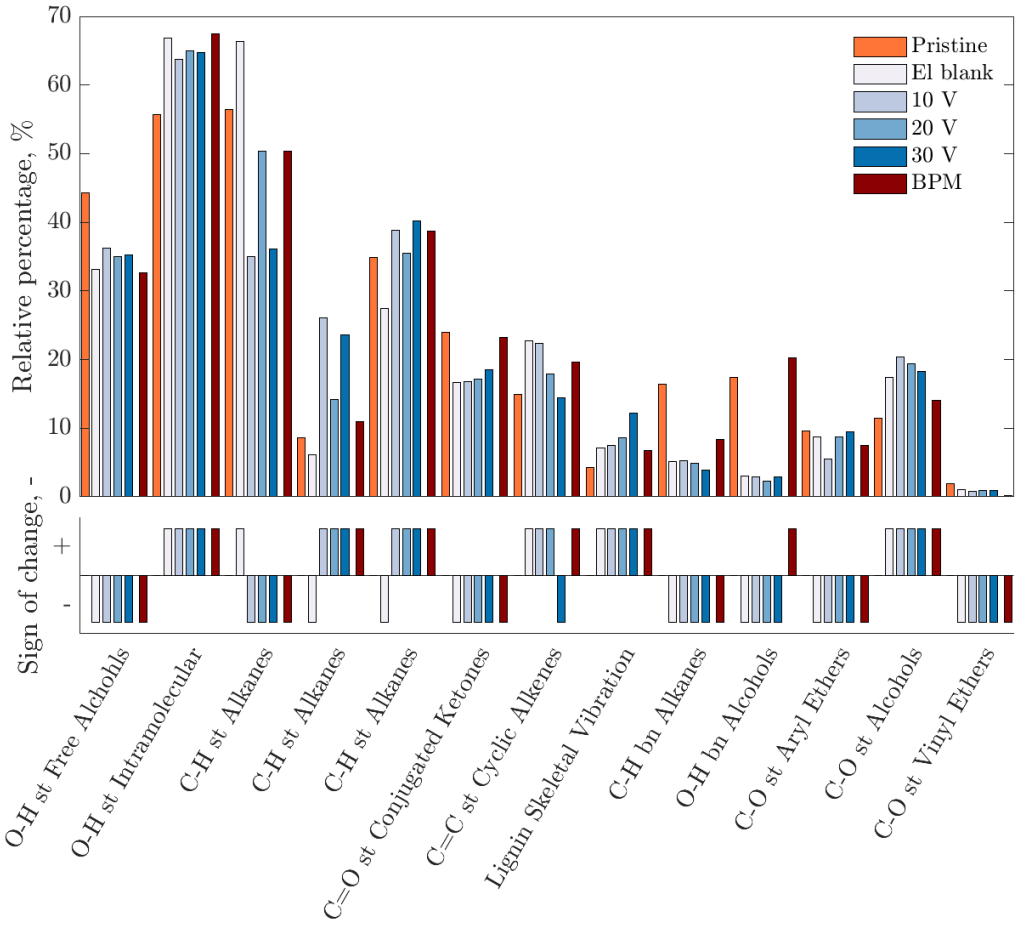

Figure S11 Upper panel: Relative percentage of the bands deconvoluted from the FTIR spectra (reported in Figure S9) of the pristine, electrochemical blank, and samples treated at 10 V, 20 V and 30 V at 200 °C. Lower panel: sign of the change with respect to the pristine BC. The deconvolution for the BPM configuration at ambient pressure and 60 °C is added for comparison (dark red).

GC-MS analysis

Figures S12 and S13 (numerical results in Table S8) report the composition in % of detectable compounds from GC-MS of the pristine biocrude, electrochemical blank, and samples treated at 10 V, 20 V and 30 V at 150 °C. For the sake of comparison the results measured at ambient pressure and 60 °C for the BPM configuration are also shown. The lower panel indicates if the peak area increased or decreased with comparison with the pristine biocrude.

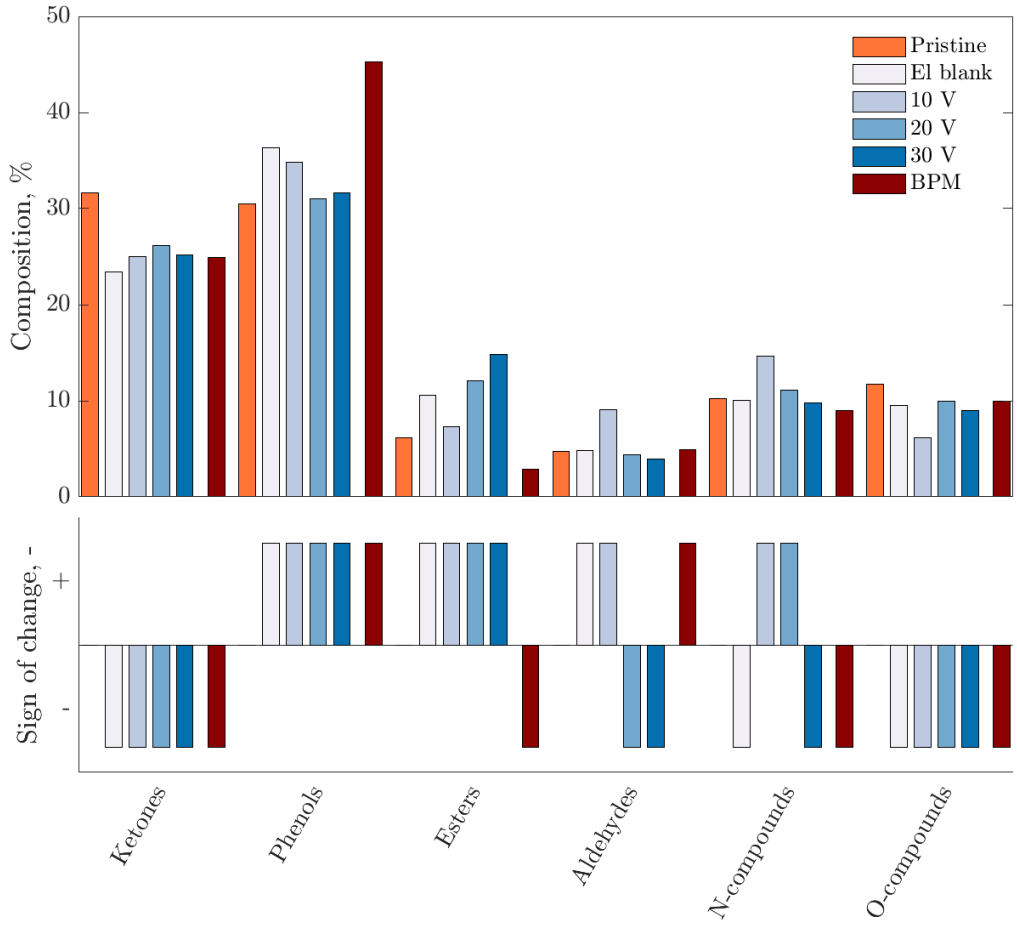

Figure S12 Upper panel: Composition of detectable compounds from GC-MS of pristine BC, electrochemical blank, and samples treated at 10 V, 20 V and 30 V at 150 °C. Lower panel: sign of the change with respect to the pristine BC. The results for the BPM configuration at ambient pressure and 60 °C are added for the sake of comparison (dark red).

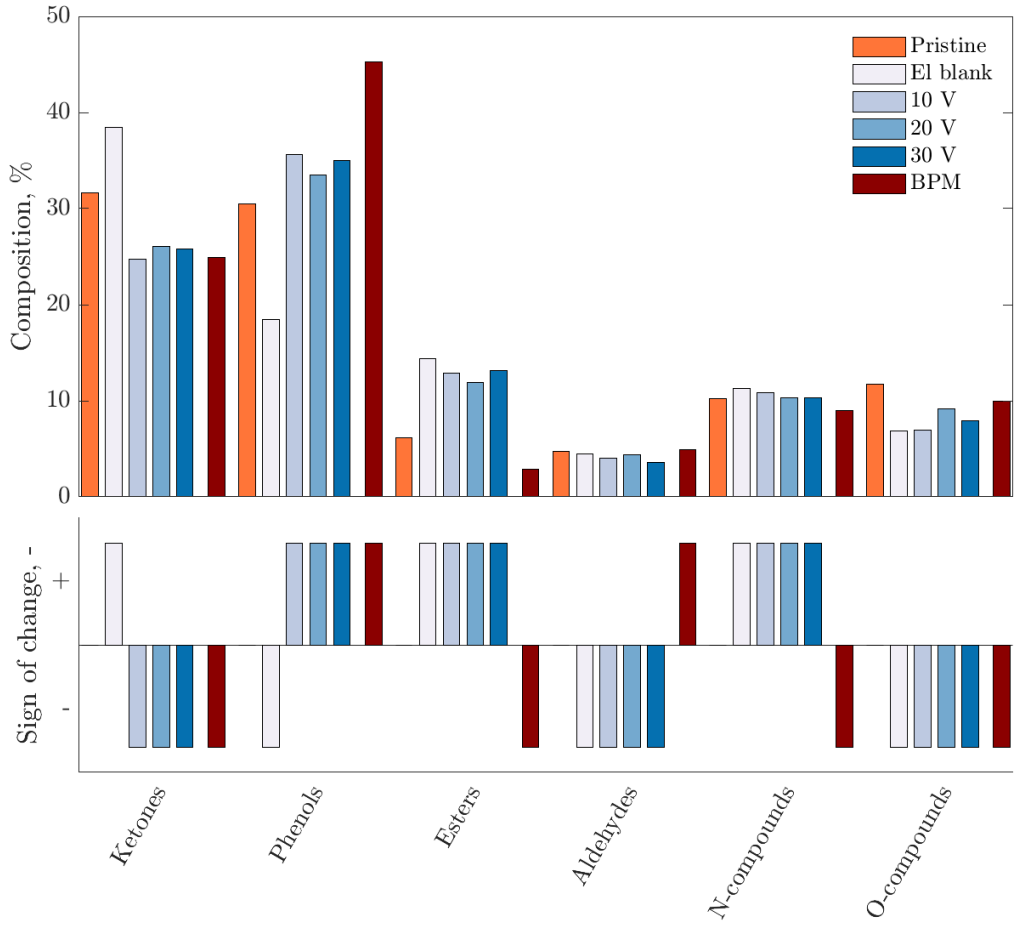

Figure S13 Upper panel: Composition of detectable compounds from GC-MS of pristine BC, electrochemical blank, and samples treated at 10 V, 20 V and 30 V at 200 °C. Lower panel: sign of the change with respect to the pristine BC. The results for the BPM configuration at ambient pressure and 60 °C are added for the sake of comparison (dark red).

Table S8. Composition of the detectable compounds from GC-MS analysis: Biocrude pristine, thermally treated (electrochemical blank), and electrochemically treated.

ΔE (V)	Q (C)	Ketones	Phenols	Esters	Aldehydes	N-compounds	O-compounds	Others
High pressure tests at 150 °C								
0	0	23.37%	36.33%	10.59%	4.83%	10.08%	9.54%	4.92%
10	72	25.00%	34.79%	7.27%	9.11%	14.66%	6.15%	3.03%
20	102	26.16%	31.05%	12.09%	4.42%	11.11%	9.95%	5.22%
30	195	25.20%	31.65%	14.79%	3.94%	9.81%	9.02%	5.60%
High pressure tests at 200 °C								
0	0	38.44%	18.49%	14.35%	4.46%	11.30%	6.82%	6.14%
10	175	24.75%	35.60%	12.92%	4.05%	10.84%	6.93%	4.92%
20	74	26.06%	33.47%	11.87%	4.34%	10.35%	9.15%	4.76%
30	420	25.82%	35.00%	13.13%	3.58%	10.35%	7.93%	4.44%

Thermal gravimetric analysis

Figure S14 reports typical TGA and DTG curves for the pristine biocrude and for the product after bulk electrolysis. A heating (N_2)-iso (N_2)-heating (air) method was used to determine the ash content of the BC residual.

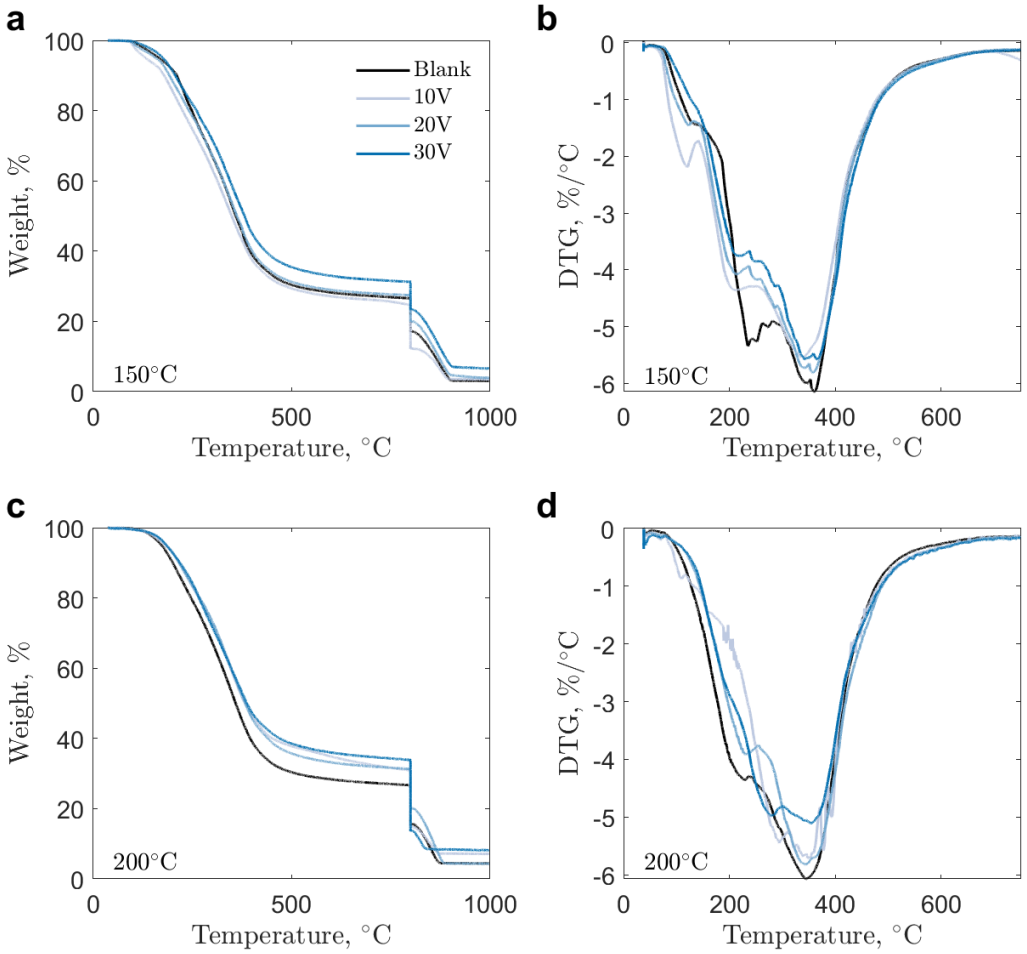

Figure S14 a TGA and **b** DTG of biocrude treated electrochemically at 150 °C; **c** TGA and **d** DTG of biocrude treated electrochemically at 200 °C. TGA temperature program: heating from 40 °C to 800 °C, 20 K/min, N_2 atmosphere; Isothermal step 4 hours at 800 °C, N_2 atmosphere; heating from 800 °C to 1000 °C, 20 K/min, in synthetic air (20% O_2).

Analysis of the process water (PW)

First we investigated the influence of the initial O_2 content for the oxidation of the organic compounds present in the process water at 200 °C. In these experiments PW was loaded in the electrochemical cell (without electrodes) and was kept at 200 °C for 2 hours. Two different initial oxygen concentrations were studied. In the first set of experiments (referred to High $c_{O_2}(0)$ in Figure S15) the initial c_{O_2} was around 5500 ppm, while in the second set (referred to Low $c_{O_2}(0)$ in Figure S15) the reactor was pressurized and depressurized in grade 5 N_2 three times before commencing the tests. In this latter case, we measured via GC analysis an initial c_{O_2} of around 200–400 ppm.

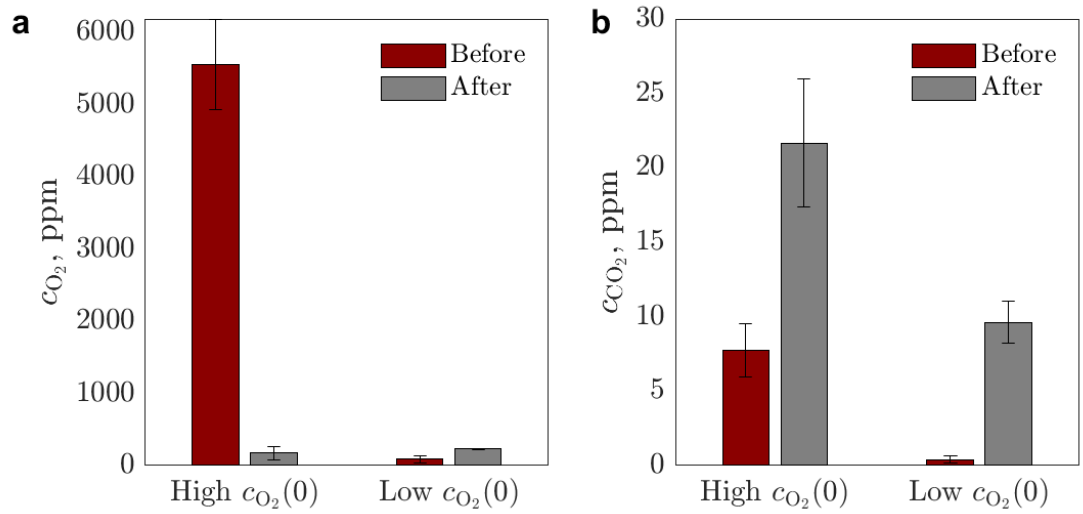

Figure S15 GC analysis of the head space in electrochemical blanks conducted at two different levels of initial O_2 concentration. The system was kept at 200 ° and around 96 bar for 2 hours. Red and grey bars represent the concentration before and after the experiment, respectively.

For all the tests, we measured the O_2 and CO_2 composition by means of GC analysis before and after the blank tests. Figure S15a shows that a very large fraction of the O_2 initially present in the head space was consumed during the blank tests when high level of O_2 were present at the beginning of the experiment. Tests performed at low O_2 concentration show a substantially unchanged level of O_2, albeit we measured a slight increase. On the other hand we found a small increase in CO_2 concentration after the blank experiments, which seemed independent

by the initial O_2 content (see Figure S15b). The results at high initial concentration of O_2 indicate the oxidation of some of the compound present in the PW; however the modest generation of CO_2 suggests only the partial oxidation of the organics on the PW. In any case, the experiments clearly show that the O_2 consumption at low initial O_2 level is negligible. All the following experiments have been carried out at low initial O_2 concentrations.

GC-MS analysis was performed on the PW after bulk electrolysis and the results of the detectable compounds are reported in Figure S16 and Table S9.

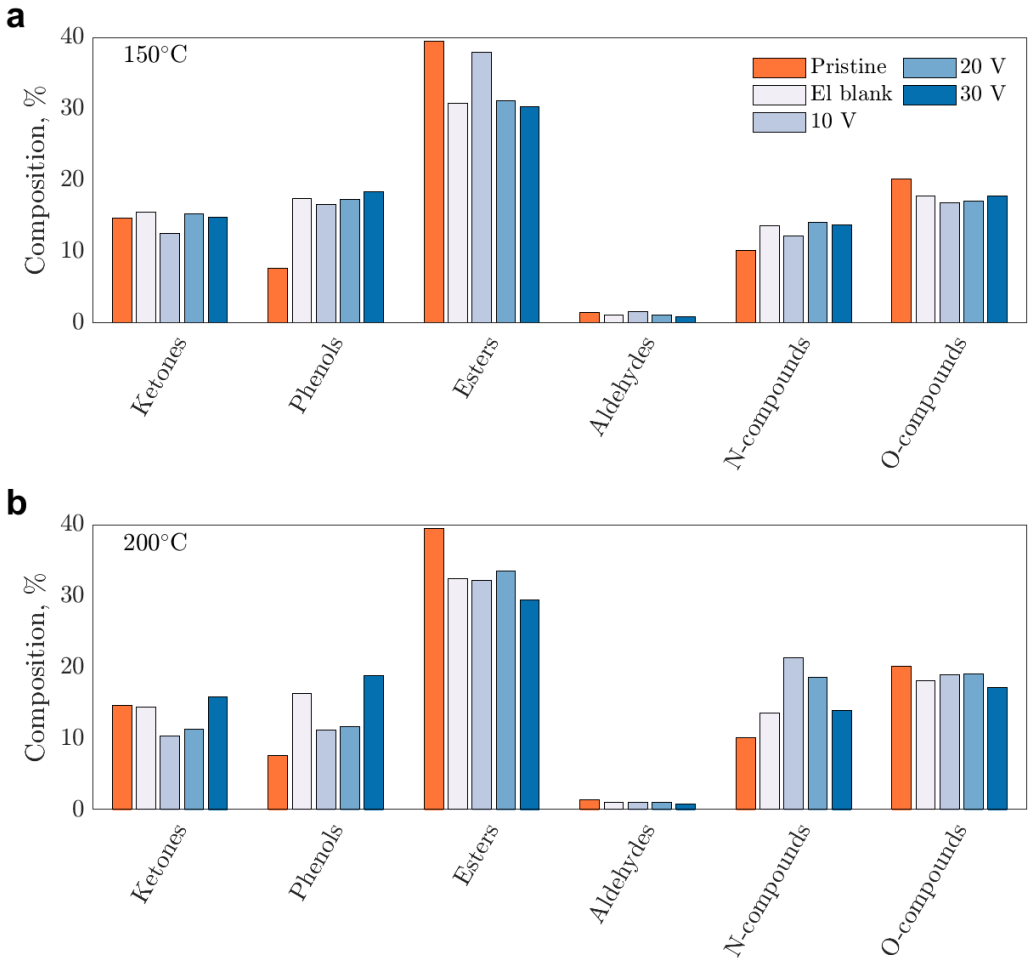

Figure S16 Composition of the detectable compounds from GC-MS analysis. Process water treated at 10 V, 20 V, and 30 V and comparison with the electrochemical blank and pristine process water. Upper panel: results for the electrolysis conducted at 150 °C. Lower panel: results for the electrolysis conducted at 200 °C.

Table S9 Composition of the detectable compounds from GC-MS analysis. Composition in percentage of the process water pristine, thermally treated (electrochemical blank) and, electrochemically treated.

Δ*E* (V)	***Q* (C)**	**Ketones**	**Phenols**	**Esters**	**Aldehydes**	**N-compounds**	**O-compounds**	**Others**
Pristine at room temperature								
0	0	14.68%	7.67%	39.51%	1.50%	10.17%	20.14%	6.33%
High pressure tests at 150 °C								
0	0	15.58%	17.48%	30.79%	1.17%	13.63%	17.75%	3.60%
10	72	12.61%	16.61%	37.95%	1.62%	12.16%	16.79%	4.75%
20	102	15.28%	17.34%	31.11%	1.11%	14.10%	17.07%	4.00%
30	195	14.84%	18.39%	30.31%	0.95%	13.78%	17.81%	3.91%
High pressure tests at 200 °C								
0	0	14.49%	16.33%	32.43%	1.16%	13.62%	18.17%	3.80%
10	175	10.42%	11.28%	32.18%	1.13%	21.42%	18.98%	4.59%
20	74	15.93%	18.81%	29.50%	0.95%	14.00%	17.22%	3.60%
30	420	15.28%	17.16%	30.29%	1.03%	15.03%	17.38%	3.84%

The results indicate a lower content of esters and a larger presence of phenols, which most probably migrate from the BC phase due to their solubility in water. The results suggest that the electrolysis does not change substantially the PW composition.

Table S10 TOC analysis of the process water pristine, thermally treated (electrochemical blank) and, electrochemically treated.

Δ*E* (*V*)	***Q* (*C*)**	**TOC (g/L)**
Pristine		
0	0	16.1
High pressure tests at 150 °C		
0	0	15.8
10	72	13.7
20	102	12.7
30	195	11.6
High pressure tests at 200 °C		
0	0	12.9
10	175	17.8
20	74	11.4
30	420	13.8

References

1. Nazari, L., Yuan, Z., Souzanchi, S., Ray, M. B. & Xu, C. (Charles). Hydrothermal liquefaction of woody biomass in hot-compressed water: Catalyst screening and comprehensive characterization of bio-crude oils. *Fuel* **162**, 74–83 (2015).
2. Meier D., Larimer D. R., & Faix, O. Direct liquefaction of different lignocellulosics and their constituents. *Fuel* **Vol 65**, (1986).
3. Cheng, S., D'cruz, I., Wang, M., Leitch, M. & Xu, C. (Charles). Highly Efficient Liquefaction of Woody Biomass in Hot-Compressed Alcohol−Water Co-solvents. *Energy Fuels* **24**, 4659–4667 (2010).
4. Derkacheva, O. & Sukhov, D. Investigation of Lignins by FTIR Spectroscopy. *Macromol. Symp.* **265**, 61–68 (2008).